THE ASTROPHYSICAL JOURNAL, 347:231–239, 1989 December 1

CO OBSERVATIONS OF THE CEPHEUS FLARE. I. MOLECULAR CLOUDS ASSOCIATED WITH A NEARBY BUBBLE

I. A. GRENIER,[1,2] F. LEBRUN,[1] M. ARNAUD,[1] T. M. DAME,[3] AND P. THADDEUS[3]

Received 1989 January 23; accepted 1989 June 8

ABSTRACT

Extended CO line emission at 2.6 mm has been mapped in the Cepheus region over 490 deg^2 at an angular resolution of 0°.5 with the Columbia 1.2 m telescope. Two molecular clouds, representing a total of 1.3×10^5 $M_\odot$, have been found above the bulk of the Local arm at a distance of 800–900 pc. The observations also reveal a vast molecular complex at $\sim$300 pc: one cloud in Cassiopeia stretches along a 30° arc and contains about 10^5 $M_\odot$, and a second at a similar distance in Cepheus contains 0.6×10^5 $M_\odot$.

The arrangement of the nearby clouds in a ring 12° in diameter, the small amount of atomic and molecular emission inside the ring, the large H I and CO velocity dispersions along its rim, and soft X-ray and radio observations all strongly suggest the presence of a hot bubble between Cepheus and Cassiopeia. As a tentative interpretation, we propose a 4×10^4 yr old Type I supernova remnant 300 pc away.

Subject headings: galaxies: The Galaxy — galaxies: structure — interstellar: molecules — nebulae: supernova remnants

I. INTRODUCTION

Hubble (1934) noticed a large region in Cepheus, well off the Galactic plane, largely free of galaxies which he named the Cepheus Flare, but no systematic study of the interstellar gas in this region was undertaken until 21 cm observations by Heiles (1967). His extensive survey ($100° \leq l \leq 140°$, $13° \leq b \leq 17°$) revealed the existence of two distinct velocity components which he interpreted as two sheets of gas extending through most of his survey region. Later, the high obscuration relative to the H I measurements in the Cepheus Flare (Strong and Lebrun 1982) prompted Lebrun (1986) to study the molecular content of the region with the Columbia 1.2 m telescope. Lebrun's CO observations revealed a large cloud covering 140 deg^2 from $l = 100°$ to 115°, $b = 11°$ to 20°; its mass and proximity make it one of the major molecular features of the solar neighborhood, similar in scale to the large clouds in Orion, though without their spectacular star formation.

This paper presents a more complete survey with the Columbia telescope of CO emission in the Cepheus region ($l = 100°$–140°, $b = 8°$–22°). These new observations cover at higher sensitivity the clouds mapped by Lebrun and extend to much higher longitude, where the presence of Heiles's two H I sheets and the high optical obscuration relative to the amount of H I (Strong and Lebrun 1982) suggested the presence of other molecular concentrations. The new data reveal a second large region of CO emission very similar in distribution to the sheets of atomic gas.

After presentation of the data, the structure and dynamics of the complex are discussed, and distances and masses for the individual clouds are estimated. Special attention is given to the emission at low velocity, because the present observations, when combined with the Columbia CO survey of the second quadrant (Dame *et al.* 1987), show that it arises from an extremely large but hitherto poorly studied object. Finally, the configuration of the local molecular clouds, which delineates an interesting loop structure, is compared to observations at other wavelengths.

A discussion of the diffuse γ-rays from the Cepheus region and their implications for the calibration of the ratio of CO to molecular hydrogen, $N(H_2)/W_{CO}$, is deferred (Grenier and Lebrun 1989, hereafter Paper II).

II. OBSERVATIONS

Observations in Cepheus of the CO $J = 1 \rightarrow 0$ transition line at 115 GHz (2.6 mm) were carried out during the winter of 1984–1985 with the 1.2 m Columbia telescope, then in New York City. To cover the Flare completely in one observing season, the full angular resolution of the antenna (8'.7 FWHM) was reduced to 0°.5 by stepping the telescope through a 4×4 square array of positions 7'.5 apart and summing the resultant spectra. A total of 1961 spectra so obtained were taken along a regular (l, b) coordinate grid that fully samples 490 deg^2 in Cepheus. Figure 1 shows the outer boundaries of the survey. No data were taken below 8° in latitude because that region was already covered by the Columbia survey of the second quadrant (Dame *et al.* 1987).

The telescope was equipped with a very sensitive, liquid helium–cooled SIS receiver with a typical single-sideband noise temperature below 90 K, and a 256 channel filter-bank spectrometer which provides a frequency resolution of 250 kHz for a velocity resolution of 0.65 km s^{-1} at 115 GHz. The filter bank was centered on 0 km s^{-1} in the local standard of rest. Emission intensities were calibrated and corrected for atmospheric absorption by briefly rotating a room-temperature blackbody wheel in front of the feed horn prior to each scan. To measure the temperature and opacity of atmospheric water vapor, antenna tipping was performed every 12 hr and more often when the weather was variable. Pointing and calibration were checked at least daily against an intense CO source near NGC 7538 ($l = 110°$, $b = 0.125°$).

Owing to the fairly wide lines observed in Cepheus and the presence of two velocity components, spectra were obtained by position-switching using two reference positions, each shown by frequency-switching to be free of CO emission to the required sensitivity. With this observing procedure, only linear

[1] Service d'Astrophysique, CEN Saclay.
[2] Centre d'Etude Spatiale des Rayonnements, Toulouse.
[3] Harvard-Smithsonian Center for Astrophysics.

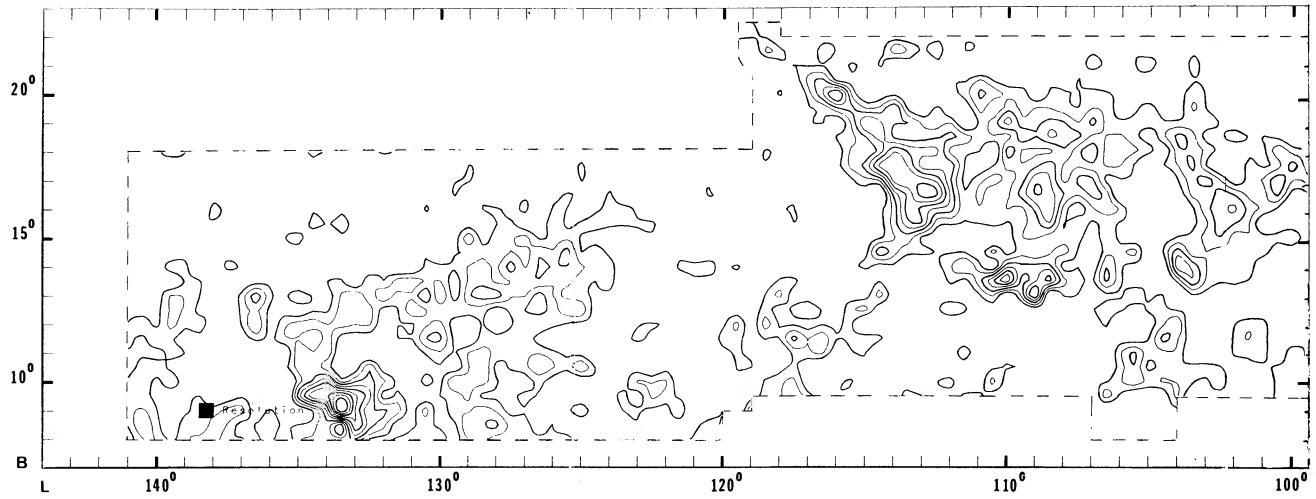

FIG. 1.—Map of ^{12}CO emission integrated over all velocities, with an angular resolution of 0°.5. The lowest contour is at 2.2 K km s^{-1}, the 2.5 σ confidence level, and the contour interval is 2.2 K km s^{-1}. The border of the survey is indicated by a dashed line.

baselines needed to be removed from the raw spectra. Integration times were set automatically to achieve a uniform rms noise of 0.2 K in radiation temperature; typical integration times on clear, cold winter days were 30–60 s.

III. RESULTS

Figure 1 presents a spatial map of W_{CO}, the CO emission integrated over all observed velocities. Both the intensity and extent of the molecular gas are far greater in the Cepheus Flare than typical at such high Galactic latitudes (see, e.g., Dame *et al.* 1987); the emission is rather similar to that found in the large clouds of Orion or Taurus. It is concentrated mainly in two regions centered near (110°, 17°) and (131°, 11°), with very little in between.

A finding chart for the optical objects in the region surveyed is shown in Figure 2. Unlike the more famous Orion and Cygnus regions, this part of Cepheus contains neither spectacular nebulae nor prominent clusters of young stars, at least outside the limited area $100° \leq l \leq 108°$, $b \leq 12°.5$ where the outskirts of Cep OB2 are found and a few small H II regions are present (S11, S133, S136, S137, S150, and S174; Marsalkova 1974), some of them already mapped in CO (Blitz, Fich, and Stark 1982). In the rest of the survey, if the molecular clouds contain newly formed stars, they must be objects of low mass, because isolated O, B, or W-R stars do not appear (Cruz-Gonzales *et al.* 1974; Van der Hucht *et al.* 1981; Humphreys 1978). Only a few T Tauri stars are found in the reflection nebulae NGC 7023 and NGC 7129, and none at all in the clouds beyond $l = 120°$ (Herbig and Rao 1972). The few faint reflection nebulae in the region (Racine 1968; Knapp *et al.* 1977) provide important distance clues. On the whole, the distribution of dust clouds, reported by Lynds (1962) or photographed by Schlosser and Görnandt (1984), agrees well with the distribution of the molecular emission.

The velocity structure of the emission is shown in Figure 3, a longitude-velocity map integrated over all latitudes observed. The partition of the emission into two parallel lanes divided by a gap near -6 km s^{-1} is characteristic of both the 21 cm and the CO emission over a large area of the second quadrant. The partition is easily seen above 120° in Figure 3, while below 120° some confusion has been introduced by the integration over latitude. However, a three-dimensional (l, b, v) representation

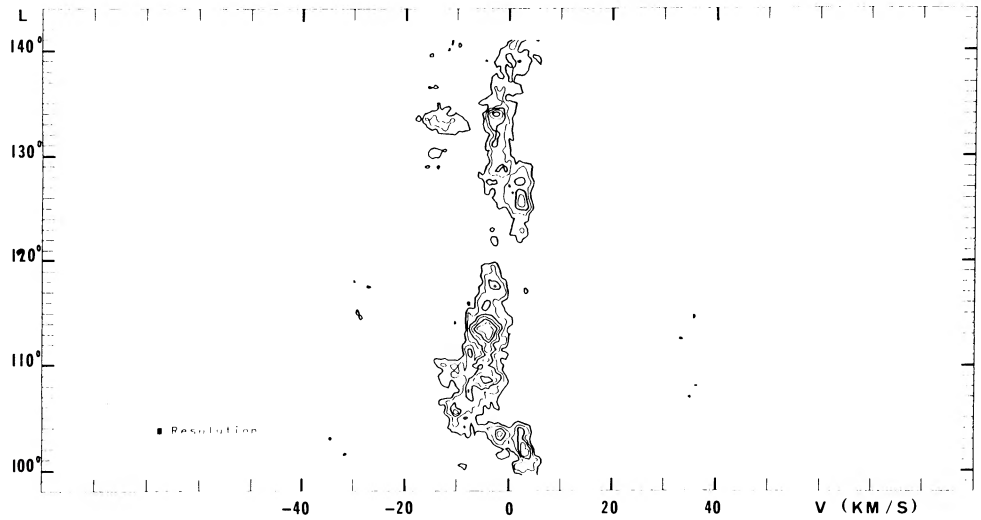

FIG. 2.—Finding chart for objects and regions discussed in the text. The W_{CO} contour sketched corresponds to the lowest contour of Fig. 1.

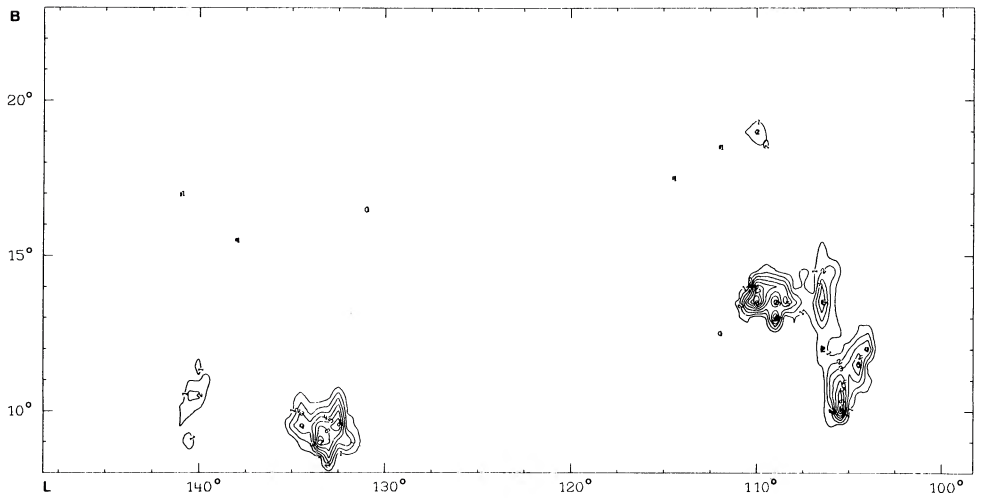

FIG. 3.—Longitude-velocity map of CO emission integrated over all latitudes surveyed. The lowest contour and interval are 1.9 K degree of latitude, and the velocity resolution is 0.64 km s^{-1}.

of the data below 120° shows an isolated cloud in the range -8 to -15 km s^{-1}, distinct from the vast cloud visible at lower velocity and higher latitude. The high-velocity component of the emission in the whole survey is displayed in Figure 4. The same velocity partition is seen in CO at lower latitudes throughout much of the second quadrant (see Fig. 3 of Dame *et al.* 1987), and a similar bifurcation is seen at 21 cm in the plane (Lindblad 1974) and at medium latitudes (Heiles 1967). In the Cepheus Flare, the close spatial and velocity correlation between the CO and the 21 cm features leaves little doubt that the two velocity components evident in Figure 3 correspond to Heiles's (1967) H I sheets. The velocity trend of the component near 0 km s^{-1} coincides with that of Lindblad's expanding H I ring, observed in the second quadrant near $b = 0°$, and with the velocity of dust clouds participating in this expansion (Sandqvist, Tomboulides, and Lindblad 1988).

a) Distances to the Two Velocity Components

Although the region surveyed contains no OB associations, there are several—Cep OB2, Cep OB3, Cep OB4, Cam OB1, and Per OB3—at lower latitude between $l = 100°$ and 150°. With distances in the range 800–1000 pc (Humphreys 1978), too close for the Perseus arm, they are plausibly related to one of the two velocity components just discussed; several studies of the CO emission toward these OB associations (e.g., Elmegreen, Dickinson, and Lada 1978; Casoli, Combes, and Gerin 1984) have shown that they are associated with the more negative velocity component at -12 km s^{-1}. A few reflection nebulae close to the Galactic plane (Rac 2 and the association Cep R 1; Racine 1968) lie in this direction between 600 and 900 pc. We therefore adopt a distance of 800 pc for the clouds at -12 km s^{-1}, in rough agreement with their admittedly very uncertain kinematic distance. A distance of 800 pc places them in the Local arm. Other optical objects probably associated with the clouds at -12 km s^{-1} in the survey are the reflection nebulae Rac 146 and Rac 143 at 1000 pc and 800 pc, respectively (Racine 1968), and the H II regions S11 and S137 at 620 pc (Blitz, Fich, and Stark 1982).

The distance of the other component, near 0 km s^{-1}, is less well determined, but its low velocity and its very large angular extent in CO and H I suggest it is significantly closer than 800 pc. Heiles estimated the two H I sheets to be at ~300 pc and ~500 pc. A number of optical objects probably associated with this nearer component are marked in Figure 2: the reflection nebulae VDB 152, DG 177, and DG 178 all have associated CO emission near -4 km s^{-1} (Knapp *et al.* 1977) and lie at distances of 400, 250, and 500 pc, respectively (Racine 1968). The brightest nebula in the region, NGC 7023, lies at 350 pc

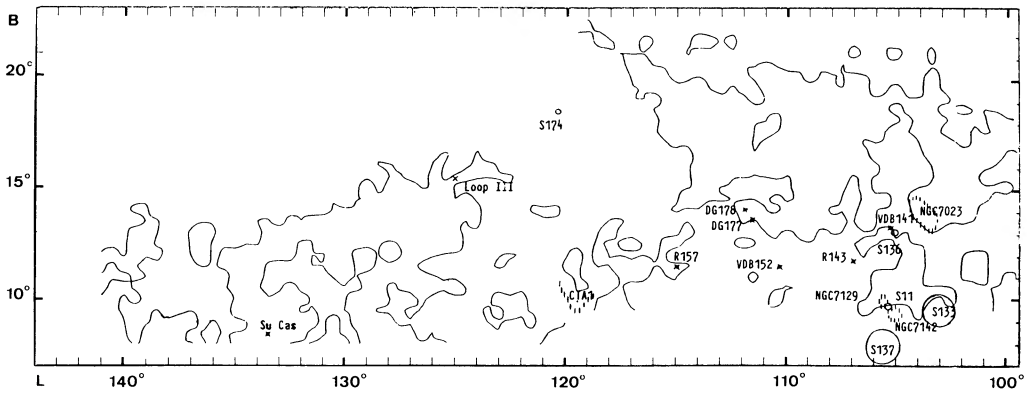

FIG. 4.—Map of CO emission from the clouds in the Local arm, i.e., integrated over velocities from -20 to -8 km s^{-1}, with an angular resolution of 0.5. The lowest contour and interval are 2 K km s^{-1}.

(Witt and Cottrell 1980) and is coincident with a strong CO emission feature with a velocity of ~ 2 km s^{-1}. The Cepheid star SU Cas and its associated reflection nebula VDB 9, also lie at a distance of 300 pc (Racine 1968). The nebulae Rac 3 and Rac 157 are found at 180 pc and 260 pc (Racine 1968). Closer to the Galactic plane, reddening measurements detect sharp absorbing fronts at ~ 300 pc and ~ 700 pc, with a faint intermediate one near 450 pc (Lucke 1978). Other measurements by Neckel and Klare (1980) lead to similar distances for the fronts. Lindblad's estimate for the distance of the H I ring in the second quadrant is 300 pc (Lindblad *et al.* 1973). On the basis of these arguments. we adopt 300 pc as the distance to the nearer component. An attempt to refine this estimate by searching for calcium and sodium lines toward A stars of known distance is currently underway; preliminary results place an absorption front at ~ 250 pc.

b) *Displacement from the Galactic Plane*

With this assignment of distances, displacements from the Galactic plane can be derived. The two clouds of the -12 km s^{-1} velocity component (Fig. 4) lie 130 pc and 170 pc above the plane. These displacements are large compared with the rms z-dispersion of all clouds within 1 kpc (74 pc; Dame *et al.* 1987), but since clouds associated with the Local arm in the second quadrant have a mean displacement of $+44$ pc (Table 2 of Dame *et al.* 1987), the clouds are not significantly displaced with respect to the bulk of the Local arm material in this direction. The nearer clouds of the survey, near 0 km s^{-1}, are displaced only 50–90 pc from the Galactic plane.

c) *Cloud Masses*

Cloud masses were computed by assuming that $N(H_2)$ is proportional to the velocity-integrated CO intensity W_{CO}. The diffuse γ-ray emission observed by the *COSB* satellite has provided so far the most reliable method of calibrating the ratio $N(H_2)/W_{CO}$ on a large scale. The value used here, (2.3 ± 1.4) 10^{20} mol cm^{-2} K^{-1} km^{-1} s, has been derived from the study of the 150–5000 MeV γ-ray flux in the Cepheus region itself (Paper II). A comparison of the γ rays and the gas content along the entire Galactic plane yields essentially the same value $(2.3 \pm 0.3 \times 10^{20}$ mol cm^{-2} K^{-1} km^{-1} s; Strong *et al.* 1988).

The molecular mass in the region of the survey using this conversion factor is $\sim 2.5 \times 10^5\ M_\odot$, which is about 6% of that within 1 kpc of the Sun (Dame *et al.* 1987). Each velocity component contains about half of the mass and, within each component, the mass is divided roughly equally between the two clouds above and below 120°, i.e., $\sim 6 \times 10^4\ M_\odot$ for each cloud.

To test whether the clouds are gravitationally bound, virial masses were calculated on the simple assumption that a cloud is a homogeneous sphere with negligible support from magnetic fields or other sources of internal pressure. Such an estimate requires knowledge of both the radius of the cloud, which we took to be (area of cloud/π)$^{1/2}$, and its composite linewidth, dv, determined from the cloud's composite line profile by assuming a Gaussian shape: dv (FWHM) $= 0.94 W_{CO}/T_{peak}$.

As expected from the relatively large velocity dispersions of the clouds (Fig. 3), the derived virial masses are systematically larger than the CO estimates (Table 1). One possible reason for the difference is that, situated relatively high above the Galactic plane, the clouds are not gravitationally bound. We explicitly assumed that only random internal motions are responsible for the velocity dispersion, but a strong velocity gradient within a cloud will cause an overestimation of the mass. This may be the case for the Cepheus clouds 3 and 5 (Table 1), for which two virial masses were calculated, one with dv derived from the total composite spectrum and the other using dv measured in different locations along the velocity gradient. In the latter case, the discrepancy between the CO and the virial masses is reduced. Below, we propose another explanation for the large virial mass of cloud 4.

d) *The Nearby Cepheus and Cassiopeia Molecular Clouds*

So far, our discussion has been limited to the CO emission found within the strict boundaries of the survey. However, in Figure 1 the emission at $l = 125°$ obviously extends to lower latitudes. Its full extent can be seen by combining our survey with the second quadrant survey of Dame *et al.* (1987). Since the same velocity bifurcation exists at lower latitudes, a map of the nearer component was produced by integrating W_{CO} from -8 to 8 km s^{-1} (Fig. 5). This nearby material extends far beyond Cepheus, well into Cassiopeia. The emission in our

TABLE 1

CHARACTERISTICS OF INDIVIDUAL CLOUDS AND OF THE CEPHEUS AND CASSIOPEIA COMPLEXES

A. INDIVIDUAL CLOUDS

Number	Longitude	Latitude	v(km s^{-1})	d(pc)	z(pc)	$M_{CO}(10^4\ M_\odot)$	M_{vir}
1	(103°, 111°)	(90°, 15°)	(−20, −8)	800	170	7.5	14
2	(131°, 135°)	(8°, 11°)	(−20, −8)	800	130	5.5	35
3	(99°.5, 104°.5)	(12°.5, 22°)	(−8, +10)	300	90	1.5	10
							3.4[a]
4	(105°, 120°)	(12°.5, 22°.5)	(−8, +10)	300	90	4.5	15
5	(122°, 141°.5)	(8°, 17°)	(−8, +10)	300	70	5.2	41
							9.5[a]
6	(114°, 121°)	(9.5°, 13°.5)	(−8, +10)	300	50	0.6	4.2

B. CEPHEUS AND CASSIOPEIA GROUPS

Name	Longitude	Latitude	v(km s^{-1})	d(pc)	z(pc)	$M_{CO}(10^4\ M_\odot)$
Cep	(100°, 120°)	(13°, 22°)	(−8, +10)	300	90	6
Cas	(114°, 143°)	(2°, 16°)	(−8, +10)	300	50	10

[a] Virial mass computed from line widths measured locally within a cloud, rather than from the cloud total composite line width.

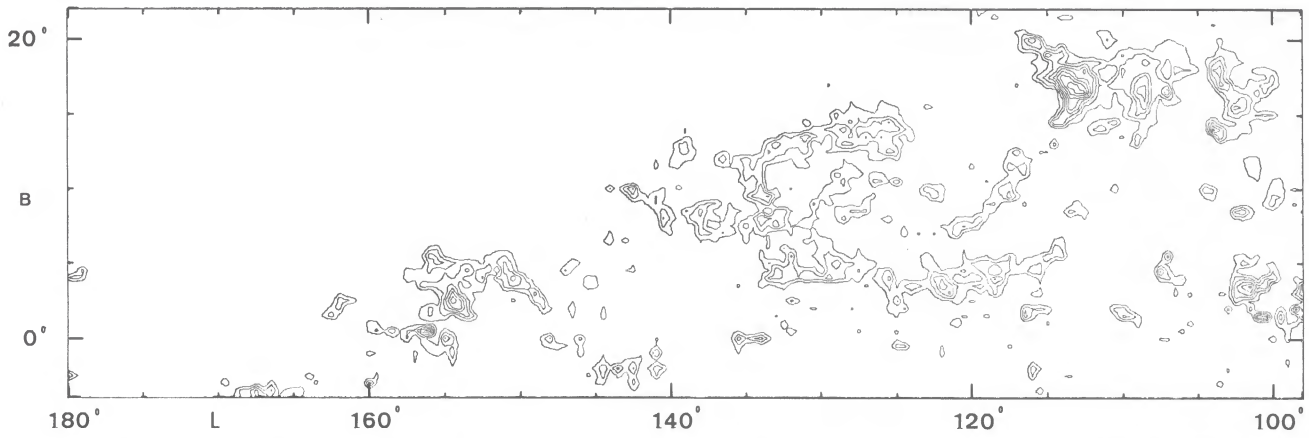

FIG. 5.—Composite map of the nearby CO emission in Cassiopeia and Cepheus, i.e., integrated from -8 to $+8$ km s^{-1}, with an angular resolution of 0°.5. The lowest contour is 3 K km s^{-1}, and the interval is 2 K km s^{-1}.

survey represents only the northern portion of a vast molecular complex delineating an arc of 30° and covering ~ 200 deg^2. For brevity, we refer to the two main concentrations of nearby material as the Cepheus cloud ($100° \leq l \leq 117°$, $13° \leq b \leq 22°$) and the Cassiopeia cloud ($115° \leq l \leq 140°$, $2° \leq b \leq 16°$).

The huge angular extent of the Cassiopeia cloud means it must lie very close to the Sun, and with a mass of $\sim 10^5\ M_\odot$ it ranks as one of the largest and most massive molecular objects in our vicinity. Another $0.6 \times 10^5\ M_\odot$ is contained in the Cepheus cloud. The difference in mass with the previous estimate of Lebrun (1986) is explained by the closer distance adopted here (300 pc instead of 450 pc) and the smaller value of $N(H_2)/W_{CO}$ recently derived (2.3 instead of 3×10^{20} mol cm^{-2} K^{-1} km^{-1} s). The masses of Cepheus and Cassiopeia are comparable to those found in Orion and Taurus. Although the projected separation of the two clouds is greater than 50 pc, since they lie at the same velocity and form an apparent loop structure on the plane of the sky (Fig. 5), they may be closely related.

Other nearby clouds (Lupus, ρ Oph, Orion, Taurus) are related to Gould's Belt. The distance and velocities of Cepheus and Cassiopeia suggest they are associated with Lindblad's H I ring and therefore participate in the expansion of the Belt. Cassiopeia and Cepheus, however, are displaced with respect to the Belt disk (50 and 90 pc, respectively). No tilt nor any warp of the Belt has been suggested (Stothers and Frogel 1974; Lucke 1978), but very few young bright stars are available above a few degrees in latitude to trace the Belt in this direction. No clues are given either to the latitude extent of the H I ring in the second quadrant (Lindblad *et al.* 1973; Lindblad 1974). So, the relationship between Cepheus, Cassiopeia, and Gould's Belt remains an open question.

e) An Old SNR between Cepheus and Cassiopeia?

The remarkable arc of the Casseiopeia cloud and the high-longitude part of Cepheus seem to delineate a broad ring which surrounds a region largely free of CO emission. Except for the small cloud around $l = 118°$, $b = 10°$ (cloud 6), the region between Cepheus and Cassiopeia above 10° is free of CO emission to a level of 0.35 K km s^{-1}. Toward Cepheus, the hole is bordered by a very sharp front where the emission drops from 18 K km s^{-1} to nearly 0 within $\sim 1°$ (i.e., within ~ 6 pc), and this front exhibits unusually wide CO lines.

Other striking aspects of the apparent ring are revealed at other wavelengths. The hole appears as a bright spot on the soft X-ray maps of the sky produced by McCammon *et al.* (1983; Figs. 6*a*–6*c*), and it is, in fact, the brightest part of the Galactic plane in the B band: 130–188 eV. A structured enhancement is also observed in the M1 band (490–930 eV) and the highest contours in the B and M1 bands nicely match the CO configuration (Fig. 7*a*). Not much structure is found in the C band (160–284 eV), yet a diffuse excess is present. The

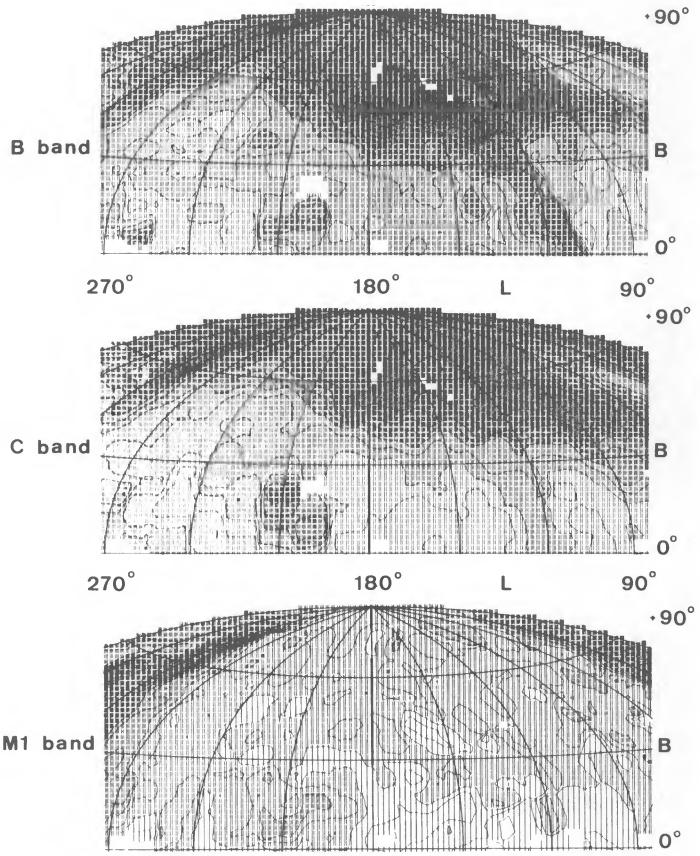

FIG. 6.—Soft X-ray flux maps of the northern Galactic anticenter from McCammon *et al.* (1983): (*a*) in the B band (130–188 eV), with a contour interval of 7.5 counts s^{-1}; (*b*) in the C band (160–284 eV), with a contour interval of 20 counts s^{-1}; and (*c*) in the M1 band (440–930 eV), with a contour interval of 5 counts s^{-1}.

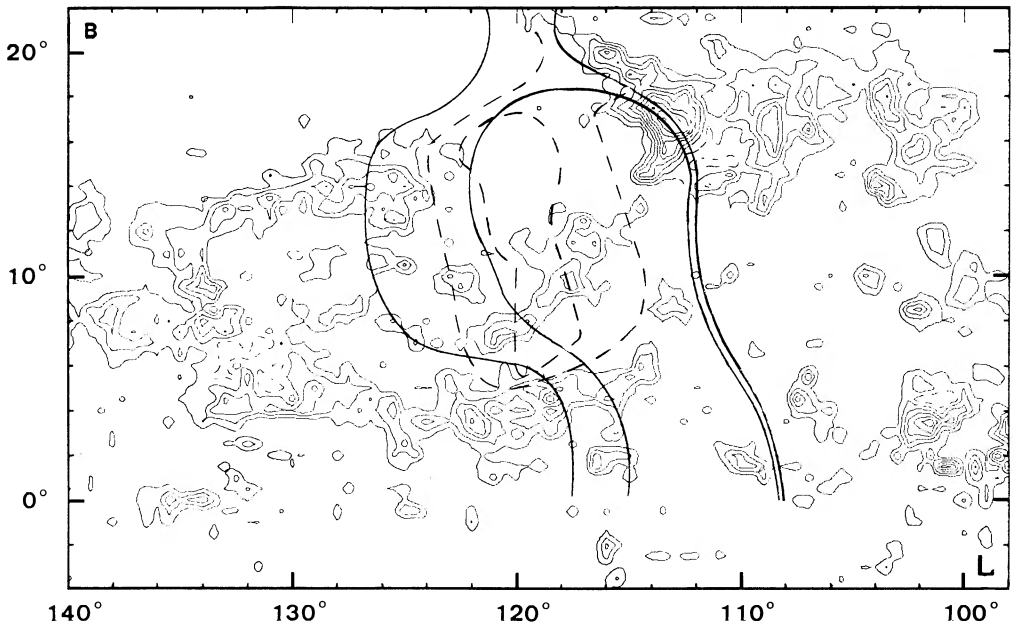

FIG. 7*a*

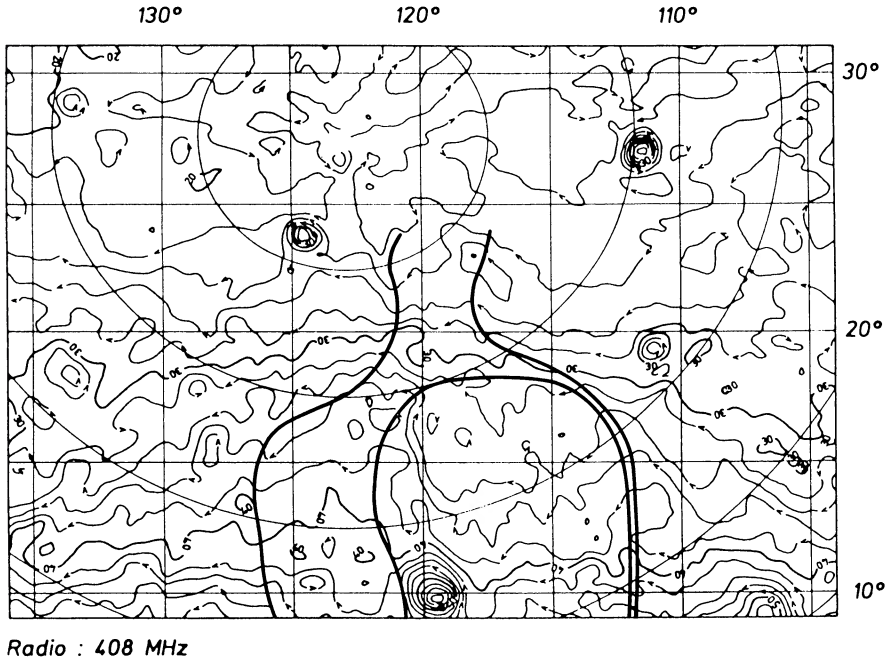

FIG. 7*b*

FIG. 7.—Observations at different wavelengths of the bubble structure: (*a*) Map of the nearby CO emission (-8; $+8$ km s^{-1}, lowest contour and interval of 2 K km s^{-1}), where the two highest contours of the soft X-ray emission in the B and M1 bands (McCammon *et al.* 1983) are indicated by thick and dashed lines, respectively. (*b*) Map of the 408 MHz radio emission from Haslam *et al.* (1981). Brightness temperatures are given on the contours. The two highest contours of the X-ray emission in the B band are indicated by thick lines.

hole is relatively depleted of atomic gas. After removing a diffuse background, Heiles (1967) found a contrast of at least a factor of 3 between the 21 cm emission inside the ring and the surrounding emission. As with the CO, the H I lines along the sharp edge of Cepheus are particularly wide. At 408 MHz (Fig. 7*c*; see also the color map of Haslam *et al.* 1981), the rim of the ring appears as a typical loop structure above 10° in latitude. The loop is coincident with the X-ray and CO structure. Below 10°, however, the radio structure vanishes into the intense Galactic emission and blends with numerous bright sources such as CTA1, W1, and S137. The radio structure can also be seen in the 820 MHz survey by Berkhuijsen (1973) and is barely visible (owing to the low angular resolution) on the 150 MHz map of Landecker and Wielebinski (1970). Remarkably, the CO, radio, X-ray, and perhaps H I structures all show a sharp edge at low longitude and a much fuzzier border at high longitude.

Owing to their softness, the X-rays must come from a nearby

source to have escaped absorption by foreground atomic gas, and the presence of the radio excess is strong evidence that the soft X-rays originate within the hole, rather than from diffuse emission behind the clouds. The relative weakness of the C band emission raises question about the reliability of the B and M1 excesses. The C band weakness is confirmed by *SAS 3* (Marshall and Clark 1984). But, since the X-ray emission in the different bands is very sensitive to the abundance of a few chemical species (Arnaud and Rothenflug 1986), a silicon depletion could explain a high B/C ratio and is plausible in an evidently dusty location. From the data at various wavelengths and their correlation, we therefore propose that a bubble of hot plasma exists between the Cepheus and Cassiopeia clouds. Its temperature must exceed a few 10^5 K, because the region does not emit Hα lines (Sivan 1974).

The Cepheus and Cassiopeia bubble is unlikely to have been blown by strong winds of young massive stars, since no such star lies in its vicinity; the only early-type stars in this direction lie well beyond, at 800–900 pc. Thus, the most plausible hypothesis is that the bubble was created by a supernova explosion.

To test this origin, the observations available were analyzed in terms of the classic Sedov's model (1959) for the evolution of SNRs. Remnants of sufficient age emit soft X-rays characterized by the energy conserved from the outburst, E, the density of the ambient interstellar hydrogen, n_0, and the shock temperature, T. Although the temperature varies within the remnant, it is relatively constant close behind the shock, where most of the mass lies, so we assumed that the temperature derived from the X-ray fluxes equals the shock temperature. The values of T and n_0 measured from the X-rays are then used in the expansion model to evaluate the energy of the explosion and its age.

The X-ray flux from the bubble was determined from the data of McCammon *et al.* (1983); since an instrumental background is probably contaminating the data (McCammon *et al.*), we have considered only the highest X-ray contours which are spatially correlated with the CO and radio structure. Subtracting the mean level of the X-ray flux in the surrounding regions (30, 40, and 10 counts s^{-1} in the B, C, and M1 bands, respectively) also attempts to remove poorly known contributions from the extragalactic background and the Local bubble. The B and M1 bands were used instead of the C band to measure the temperature, because they are stronger and better correlated with the ring structure seen at other wavelengths. With the curves of McCammon *et al.*, which give count rates expected from a hot plasma (with solar abundances and in thermal equilibrium) as a function of its emission measure and temperature, the ratio B/M1 yields a temperature of 1.5×10^6 K and an emission measure of 10^{-2} cm^{-6} pc. To take into account the weakness of the C band emission, two extreme cases have been determined using the B/C and C/M1 ratios which yield temperatures of 0.5 and 2.2×10^6 K and emission measures of 1.5 and 0.35×10^{-2} cm^{-6} pc. Thus, the supernova event has been tested in all three cases. Its characteristics have been estimated from Sedov's equations (Hamilton, Sarazin, and Chevalier 1983):

$$E = n_0 \left(\frac{T}{10^7\ \mathrm{K}}\right)\left(\frac{r}{8.62\ \mathrm{pc}}\right)^3 10^{51}\ \mathrm{ergs}\ ,$$

$$v = 839\left(\frac{T}{10^7\ \mathrm{K}}\right)\ \mathrm{km\ s^{-1}}\ ,$$

$$a = 4015\left(\frac{T}{10^7\ \mathrm{K}}\right)^{-0.5}\left(\frac{r}{8.62\ \mathrm{pc}}\right)\ \mathrm{yr}\ ,$$

$$M = 96.8\left(\frac{T}{10^7\ \mathrm{K}}\right)^{-1}\left(\frac{E}{10^{51}\ \mathrm{ergs}}\right) M_\odot\ ,$$

where E is the remnant's total energy, v is its present expansion velocity, a is its age, and M is the swept-up interstellar mass. At a distance d of 300 pc, the radius of the bubble, r, is taken to be 30 pc. The density of the ambient interstellar hydrogen, n_0, is related to the emission measure, EM, by the equation:

$$\mathrm{EM} = \frac{\int_0^r n_e^2(l) l^2 dl}{4\pi d^2} \approx \frac{{n_0}^2 r^3}{d^2}\ ,$$

where n_e is the electron density within the remnant.

The results for the three cases are listed in Table 2. Since the remnant is undoubtedly old, the pure adiabatic expansion may be irrelevant. The remnant may have reached the phase when radiative losses become important. This was tested by calculating the critical size at which the radiative phase begins. According to Kahn (1975),

$$R_c = 53\left(\frac{E}{10^{52}\mathrm{ergs}}\right)^{2/7}\left(\frac{n_0}{0.427\ \mathrm{cm^{-3}}}\right)^{-3/7}\ \mathrm{pc}\ .$$

The values found for R_c indicate that the bubble has not yet reached this state, although it is close to it. Thus, the application of Sedov's model is still a reasonable approximation.

TABLE 2

CHARACTERISTICS OF THE SUPERNOVA REMNANT

CHARACTERISTIC	X-RAY BAND		
	B and C	B and M1	C and M1
Temperature[a] (K)	0.5×10^6	1.5×10^6	2.2×10^6
Emission measure[a] (cm^{-6} pc)	1.5×10^{-2}	1.0×10^{-2}	0.3×10^{-2}
Ambient ISM density[a] (cm^{-3})	0.2	0.2	0.1
Expansion velocity[b] (km s^{-1})	190	320	390
Conserved energy[b] (ergs)	0.5×10^{51}	1.2×10^{51}	1.0×10^{51}
Present age[b] (yr)	6.2×10^4	3.6×10^4	3.0×10^4
Swept-up ISM mass[b] ($M_\odot$)	900	750	450
Radiative phase radius[b] (pc)	30	40	50

[a] Derived from the X-ray measurements.
[b] From Sedov's equations.

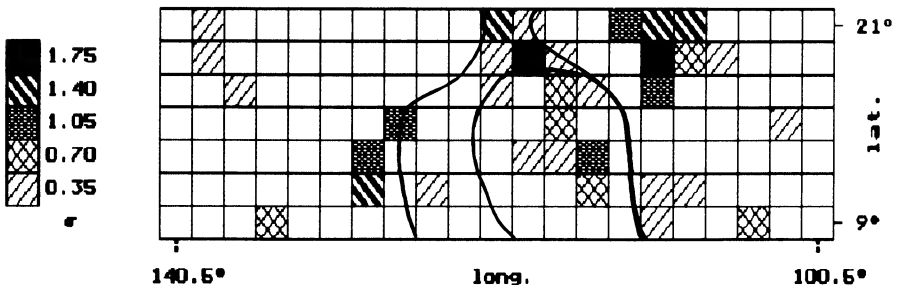

FIG. 8.—Excesses measured in 2° × 2° bins between the γ-ray emission *observed* at 70–150 MeV and *predicted* in this range from the gas column-density and an average γ-ray emissivity for the gas. Only excesses above +0.3 σ are shown.

All parameters listed in Table 2 must be considered order-of-magnitude estimates owing to the large uncertainties in the measurements. The distance of the bubble and the absorption of the X-rays are crucial: the extreme cases presented here span the range of uncertainty of the X-ray measurements, and varying the distance from 250 to 500 pc does not affect the order of magnitude of the energy output and the age of the event, varying as $d^{2.5}$ and d, respectively. Over all, the bubble observed is consistent with a 4×10^4 yr-old supernova releasing 10^{51} ergs into the ambient medium. Its total energy output is consistent with a Type I supernova. Such an age is reasonable: if the supernova were younger than a few thousand years, it would probably have been recorded historically since it was probably very conspicuous (a visual magnitude of −11 to −12); if older than a few times 10^5 yr, it would have vanished into the interstellar medium. The supernova hypothesis is statistically reasonable, because the number of SNRs younger than 10^5 yr expected within 500 pc is of order a few, if the rate of supernovae in the Galaxy is $(30 \text{ yr})^{-1}$. A crude estimate of the spectral index of the radio emission measured along the bubble's rim at 408 and 820 MHz yields −2.2, similar to the indices of other well-known remnants.

The radio loop at 408 and 820 MHz seems nonthermal, indicating the presence of a synchrotron-emitting gas behind the shock. Gamma-ray observations are of interest in this context. One would expect the electrons responsible for the radio emission to emit γ rays by bremsstrahlung with the compressed gas (Blandford and Cowie 1982). The ratio of γ-ray flux to synchrotron flux should be highest where the shock travels through a dense molecular cloud, owing to the low compression of the gas (and magnetic field) (Pollock 1985). The γ-ray intensities observed by *COS B* have been compared to the intensities predicted from the gas content of the region (using average γ-ray emissivities derived for the gas in the solar neighborhood; see Paper II). Figure 8 shows the regions where the observed γ-ray emission in the range 70–150 MeV is larger than expected from the gas content. A weak but systematic excess appears along the rim of the bubble, particularly at low longitude. Since the effect is marginal (3.4 σ), new observations which might confirm its existence would be highly desirable. The absence of an enhancement above 150 MeV is consistent with a bremsstrahlung origin for the γ rays.

As a final remark, supernova shells are not rare in this part of the solar neighborhood. Hu (1981) has observed a large H I bubble at $l = 105°$, $b = 17°.5$, which she places at ∼500 pc, with a radius of ∼26 pc. Another H I shell in the region interpreted as a 10^6 yr old SNR (Velden and Hirth 1982) is found toward $l = 130°$, $b = 22°.5$, at a kinematic distance of 450 pc with a radius of 24 pc. Further, the radio bubble Loop III dominates the second quadrant. To account for the radio flux and polarization measurements along the spur, Spoelstra (1972) placed the center of Loop III toward (125°, 115°.5) at 150 pc from the Sun. This position and the observed angular radius of 45° imply that the shock front is very close to the Cepheus and Cassiopeia clouds, but, again, the uncertainties in the distances are too large to say whether Loop III is actually disturbing these clouds.

V. CONCLUSION

The present CO observations reveal two large clouds with masses of 6 and 8×10^4 $M_\odot$ in a high-elevation region of the Local arm at 800 pc, as well as a very large complex in the solar vicinity: the Cassiopeia cloud containing $\sim 10^5$ $M_\odot$ and lying ∼300 pc from the Sun and, at about the same distance, another massive and possibly related object, the Cepheus cloud, containing 0.6×10^5 $M_\odot$.

The relation of the Cassiopeia and Cepheus clouds to Gould's Belt is unclear. Their velocities suggest a relationship to Lindblad's H I expanding ring of the Belt, yet they are found well above the position of the Belt. A careful study in the second quadrant of the latitude extent of both this expanding ring and the distribution of young massive stars might clarify the situation. Are the Cassiopeia and Cepheus clouds linked to the Belt? Is the Belt slightly tilted toward Cepheus (even a few degrees would be enough)? Or might it have been tilted in the past (i.e., it may have a seesaw motion perpendicular to the Galactic plane; Frogel and Stothers 1977)?

A bubble appears to exist between the Cassiopeia and Cepheus clouds which is very bright in soft X-rays and is bordered by a radio loop seen at 408 MHz and 820 MHz. The bubble is visible at many wavelengths (at 408 MHz, in the B and M1 X-ray bands, in CO, and perhaps in H I) and is particularly distinct along the sharp front of the Cepheus cloud, where the CO and H I lines are unusually wide. Most probably filled with a hot plasma, it cannot have been formed by a stellar wind, because no young massive star has been found inside it. All the observations are consistent with a 4×10^4 yr old SNR with an energy of 10^{51} ergs, located 300 pc from the Sun. The existence of such a supernova bubble implies a link between the Cassiopeia and Cepheus clouds and would also explain the wide lines observed in the Cepheus cloud, as the result of shocks.

Further observations at many wavelengths are required to confirm the supernova origin of the bubble. New, precise X-ray measurements would be valuable in studying the physical con-

ditions inside the remnant. Radio surveys at different frequencies are needed to remove the thermal Galactic emission and improve the loop contrast, allowing an analysis of the synchrotron emission. An estimate of the magnetic field strength is required to evaluate the density of the electrons behind the shock that cause the radio and maybe γ-ray emission. At optical wavelengths, filaments can be searched for, while in the infrared it would be extremely interesting to detect shocked hydrogen lines from the Cepheus cloud being overtaken by the blast wave of the SN. Gamma-ray data from the Sigma, Gamma-I, and GRO satellites will confirm and quantify the high-energy emission from the shocked region.

If confirmed, this nearby supernova remnant would be extremely valuable for refining theoretical models of remnants near the radiative phase and would provide an excellent example of a dense molecular cloud interacting with a supernova shock.

We are grateful to E. Sarot for editorial assistance and to J. Montani for his help with the observations.

REFERENCES

Arnaud, M., and Rothenflug, R. 1986, *Adv. Space Res.*, **6**, 119.
Berkhuijsen, E. M. 1973, *Astr. Ap.*, **24**, 143.
Blandford, R. D., and Cowie, L. L. 1982, *Ap. J.*, **260**, 625.
Blitz, L., Fich, M., and Stark, A. A. 1982, *Ap. J. Suppl.*, **49**, 183.
Casoli, F., Combes, F., and Gerin, M. 1984, *Astr. Ap.*, **133**, 99.
Cruz-Gonzales, C., Recillas-Cruz, E., Costero, R., Peimbert, M., and Torres-Peimbert, S. 1974, *Rev. Mexicana Astr. Ap.*, **1**, 211.
Dame, T. M., *et al.* 1987, *Ap. J.*, **322**, 706.
Elmegreen, B. G., Dickinson, D. F., and Lada, C. J. 1978, *Ap. J.*, **220**, 853.
Frogel, J. A., and Stothers, R. 1977, *A.J.*, **82**, 890.
Grenier, I. A., and Lebrun, F. 1989, *Ap. J.*, submitted (Paper II).
Hamilton, A. J. S., Sarazin, C. L., and Chevalier, R. A. 1983, *Ap. J. Suppl.*, **51**, 115.
Haslam, C. G. T., Salter, C. J., Stoffel, H., and Wilson, W. E. 1981, *Astr. Ap. Suppl.*, **41**, 1.
Heiles, C. 1967, *Ap. J.*, **149**, 97.
Herbig, G. H., and Rao, K. 1972, *Ap. J.*, **174**, 401.
Hu, E. 1981, *Ap. J.*, **248**, 119.
Hubble, E. P. 1934, *Ap. J.*, **79**, 8.
Humphreys, R. M. 1978, *Ap. J. Suppl.*, **38**, 309.
Kahn, F. D. 1975, *Proc. 14th Int. Cosmic Ray Conf.*, Munich, **11**, 3566.
Knapp, G. R., Kuiper, T. B. H., Knapp, S. L., and Brown, R. L. 1977, *Ap. J.*, **214**, 78.
Landecker, T. L., and Wielebinski, R. 1970, *Australian J. Phys. Ap. Suppl.*, **16**, 1.
Lebrun, F. 1986, *Ap. J.*, **306**, 16.
Lindblad, P. O. 1974, *Highlights Astr.*, **3**, 381.
Lindblad, P. O., Grape, K., Sandqvist, Aa., and Schober, J. 1973, *Astr. Ap.*, **24**, 309.
Lucke, P. B. 1978, *Astr. Ap.*, **64**, 367.
Lynds, B. T. 1962, *Ap. J. Suppl.*, **7**, 1.
Marsalkova, P. 1974, *Ap. Space Sci. Rev.*, **27**, 3.
Marshall, F. J., and Clark, G. W. 1984, *Ap. J.*, **287**, 633.
McCammon, D., Burrows, D. N., Sanders, W. T., and Kraushaar, W. L. 1983, *Ap. J.*, **269**, 107.
Neckel, Th., and Klare, G. 1980, *Astr. Ap. Suppl.*, **42**, 251.
Pollock, A. M. T. 1985, *Astr. Ap.*, **150**, 339.
Racine, R. 1968, *A.J.*, **73**, 233.
Sandqvist, Aa., Tomboulides, H., and Lindblad, P. O. 1988, *Astr. Ap.*, **205**, 225.
Schlosser, W., and Görnandt, V. 1984, *Astr. Ap.*, **137**, 287.
Sedov, M. 1959, *Similarity and Dimensional Methods in Mechanics* (New York: Academic).
Sivan, J.-P. 1974, *Astr. Ap. Suppl.*, **16**, 163.
Spoelstra, T. A. T. 1972, *Astr. Ap.*, **21**, 61.
Stothers, R., and Frogel, J. A. 1974, *A.J.*, **79**, 456.
Strong, A. W., *et al.* 1988, *Astr. Ap.*, **207**, 1.
Strong, A. W., and Lebrun, F. 1982, *Astr. Ap.*, **105**, 159.
Van der Hucht, K. A., Conti, P. S., Lundström, I., and Stenholm, B. 1981, *Space Sci. Rev.*, **28**, 227.
Velden, L., and Hirth, W. 1982, *Astr. Ap.*, **113**, 340.
Witt, A. N., and Cottrell, M. J. 1980, *A.J.*, **85**, 22.

M. Arnaud, I. Grenier, and F. Lebrun: Service d'Astrophysique, Centre d'Etudes Nucléaires de Saclay, 91191 Gif sur Yvette Cedex, France

T. Dame and P. Thaddeus: Harvard-Smithsonian Center for Astrophysics, 60 Garden Street, Cambridge, MA 02138